Metadata of the chapter that will be visualized online

Chapter Title	Luminescence of Er^{3+} Ions in Nanocrystalline Glass-Ceramics	
Copyright Year	2016	
Copyright Holder	Springer Science+Business Media Dordrecht	
Corresponding Author	Family Name	**Balda**
	Particle	
	Given Name	**Rolindes**
	Suffix	
	Division	Departamento de Física Aplicada I, Escuela Superior de Ingeniería
	Organization	Universidad del País Vasco UPV/EHU, Alda. Urquijo s/n 48013 Bilbao, Spain and Materials Physics Center CSIC-UPV/EHU
	Address	20080, San Sebastián, Spain
	Email	rolindes.balda@ehu.es
Author	Family Name	**Morea**
	Particle	
	Given Name	**R.**
	Suffix	
	Division	Laser Processing Group
	Organization	Instituto de Optica, CSIC
	Address	Serrano 121, 28006, Madrid, Spain
Author	Family Name	**Gonzalo**
	Particle	
	Given Name	**J.**
	Suffix	
	Division	Laser Processing Group
	Organization	Instituto de Optica, CSIC
	Address	Serrano 121, 28006, Madrid, Spain
Author	Family Name	**Fernandez**
	Particle	
	Given Name	**J.**
	Suffix	
	Division	Departamento de Física Aplicada I, Escuela Superior de Ingeniería
	Organization	Universidad del País Vasco UPV/EHU, Alda. Urquijo s/n 48013 Bilbao, Spain

and Materials Physics Center CSIC-UPV/EHU
Address 20080, San Sebastián, Spain
Email joaquin.fernandez@ehu.es

Abstract

This work analyzes the influence of the nanocrystals on the luminescence properties of Er^{3+} ions in transparent oxyfluoride tellurite glass-ceramics obtained by heat treatment of the precursor Er-doped glass. The comparison between the fluorescence properties of Er-doped glass and glass-ceramic suggests that a fraction of Er^{3+} ions are forming nanocrystals while the rest remain in a glass environment. The presence of ErF_3 nanocrystals has a strong effect in the upconverted red emission from $^4F_{9/2}$ level. The time evolution of the upconverted red emission shows that energy transfer upconversion processes are responsible for the increase of this emission in the glass-ceramic sample.

Chapter 15
Luminescence of Er^{3+} Ions in Nanocrystalline Glass-Ceramics

Rolindes Balda, R. Morea, J. Gonzalo, and J. Fernandez

Abstract This work analyzes the influence of the nanocrystals on the luminescence properties of Er^{3+} ions in transparent oxyfluoride tellurite glass-ceramics obtained by heat treatment of the precursor Er-doped glass. The comparison between the fluorescence properties of Er-doped glass and glass-ceramic suggests that a fraction of Er^{3+} ions are forming nanocrystals while the rest remain in a glass environment. The presence of ErF_3 nanocrystals has a strong effect in the upconverted red emission from $^4F_{9/2}$ level. The time evolution of the upconverted red emission shows that energy transfer upconversion processes are responsible for the increase of this emission in the glass-ceramic sample.

15.1 Introduction

Rare earth-doped transparent oxyfluoride glass-ceramics have been the subject of several recent investigations since they possess optical properties of interest for photonic applications such as lasers, optical amplifiers, sensors, light converters and so on. In particular, these materials containing one or more crystalline phases embedded in the glass matrix, combine the low phonon energy, optical transparency and rare-earth (RE) ions solubility of fluoride crystals with the good mechanical, thermal, and chemical properties of oxide glasses [1].

The first transparent glass-ceramic (TGC) based on aluminosilicate glass doped with Er^{3+} and Yb^{3+} ions was developed by Wang & Ohwaki in 1993 [2]. In this glass, cadmiun lead fluoride nanocrystals were nucleated by suitable thermal treatments. It was observed that, exciting Yb^{3+} ions at 970 nm, the green-red upconversion emission from Er^{3+} ions was 100 times more intense than observed

R. Balda (✉) • J. Fernandez
Departamento de Física Aplicada I, Escuela Superior de Ingeniería, Universidad del País Vasco UPV/EHU, Alda. Urquijo s/n 48013 Bilbao, Spain and Materials Physics Center CSIC-UPV/EHU, 20080 San Sebastián, Spain
e-mail: rolindes.balda@ehu.es; joaquin.fernandez@ehu.es

R. Morea • J. Gonzalo
Laser Processing Group, Instituto de Optica, CSIC, Serrano 121, 28006 Madrid, Spain

B. Di Bartolo et al. (eds.), *Nano-Optics: Principles Enabling Basic Research and Applications*, NATO Science for Peace and Security Series B: Physics and Biophysics, DOI 10.1007/978-94-024-0850-8_15

from fluoride glass, which suggested the segregation of Yb^{3+} and Er^{3+} ions in the nanocrystals. Since then, different rare earth doped oxyfluoride glass ceramics mainly based on silicate glass matrices and other fluoride crystal phases, such as LaF_3 [3–5], CaF_2 [6, 7], BaF_2 [8, 9], etc. have been proposed as active media for solid state lasers, optical amplifiers, phosphors or to enhance the efficiency of photovoltaic cells [10, 11]. However, the limited RE solubility of silica-based compositions and small nonlinear behavior as well as the low chemical durability of pure fluoride compositions has motivated the search for other glass precursors for TGC.

Among different oxide glasses, tellurite glasses combine good mechanical stability, chemical durability, and high linear and nonlinear refractive indices, with a wide transmission window (typically 0.4–6 μm), which make them promising materials for photonic applications [12]. In fact, broadband Er-doped fiber amplifiers have been achieved by using tellurite-based fibers with a gain of 25.3 dB and a noise figure of less than 6 dB from 1561 to 1611 nm [13] and more recently, efficient laser emission around 2 μm has been demonstrated in a tellurite fiber doped with Tm^{3+} ions [14].

Mixed fluorotellurite glasses which combine the low phonon energies of fluorides with the high chemical durability and thermal stability of tellurites can reduce the OH content which has a great influence in the quenching processes of the radiative emission of excited levels of rare earth ions, which increases fluorescence lifetimes [15, 16]. The transformation, by the adequated heat treatment, of flurotellurite glasses into glass-ceramics in which the RE ions are incorporated in the crystalline phase can increase the maximum cross-sections of the RE ions and the emission efficiency. However, up to now, there are only a few works dealing with Er^{3+}-doped fluorotellurite glass ceramics [17, 18].

In this work, we report the effect of the heat treatment on absorption spectra, near infrared luminescence, and upconversion emission of Er^{3+}-doped transparent oxifluoride tellurite glass-ceramics obtained by the heat treatment of the Er^{3+}-doped 73.6 TeO_2–17.6 ZnO–8.8 ZnF_2 glass. The comparison of the fluorescence properties of Er^{3+}-doped precursor glass and glass-ceramic confirms the successful incorporation of the rare-earth into the nanocrystals.

15.2 Theoretical Background

The rare-earth ions, referred to as the lanthanides, comprise the series of elements in the sixth row of the periodic table after lanthanum from cerium to ytterbium. These atoms are usually incorporated in crystalline or amorphous hosts as trivalent ions and occasionally as divalent ions. The ground state configuration of the trivalent rare-earth ions is $[Xe]4f^n$ where n varies from 1 (Ce^{3+}) to 13 (Yb^{3+}) and indicates the number of electrons in the unfilled 4f shell.

The 4f electrons are shielded by external full outer shells which limits the interaction between the ion and the crystalline field to a small perturbation giving the RE ions their characteristic sharp and well defined spectral features.

The optical activity of the RE ions in solids occurs mainly between electronic states within the 4f configuration. These transitions are parity forbidden and are made partially allowed by crystal field interactions mixing states of different parity. The result is that the transitions between 4f states are weak, with oscillator strengths of the order of 10^{-6}, and radiative lifetimes in the micro and miliseconds range. The long lifetime plays an important role to increase the probability of sequential excitations in the excited states of a single ion as well as in permitting ion-ion interactions in the excited states to allow energy transfer.

The lifetime of an emitting level is governed by a sum of probabilities for several competing processes: radiative decay, nonradiative decay by multiphonon (MPH) relaxation and by energy transfer to other ions. MPH relaxation processes in which the energy difference between the emitting level and the next lower level is converted into many lattice phonons are strongly dependent on the host matrix. Generally, the larger the number of phonons needed to convert the excitation energy, the lower is the efficiency of the non radiative processes. Therefore to enhance the emission efficiency hosts with low phonon energy are required.

Energy levels in rare-earth ions are labeled according to their angular momentum and spin quantum numbers using terms symbols such as $^4I_{15/2}$, or $^4S_{3/2}$. Here the letter refers to the total orbital angular momentum of the ion, the superscript is the number of possible orientation of the total spin of the ions, given as $2S + 1$, where S is the total spin angular momentum. The subscript refers to the total angular momentum of the ion and is determined using the Russell-Saunders coupling scheme [19]. These levels represent the energy levels of a free ion. However, when the ion is in a host, electron-host interactions further split these levels into Stark sublevels, due to the effect of the electric field of the matrix (crystal field effect). This effect is quite small since the 4f orbitals are shielded from the environment by the filled 5s and 5p sub-shells. Nevertheless, the crystal field (CF) induced by the host is what determines the shape of the absorption and emission spectra of RE ions. When comparing the spectra of RE ions in crystals and glasses, the absorption and emission bands are narrow with well resolved Stark components, even at room temperature, in the case of crystals when RE ions occupy a well defined crystal field site. On the contrary, the spectra of RE ions in an amorphous matrix, like a glass, present an inhomogeneous broadening due to the different sites occupied by the ions in the host and thus, different crystal fields. As a consequence the Stark structure of RE spectra in glasses is only partially resolved even at low temperature.

On the other hand, the symmetry and strength of the CF also affect the splitting of the levels. Moreover, the probability of radiative and nonradiative transitions is strongly affected by the host matrix.

The radiative transition probabilities between energy levels in rare-earth ions can be calculated by using the Judd-Ofelt theory [20, 21]. In the framework of this

theory, and considering the electric-dipole and magnetic-dipole contributions, the radiative transitions within the $4f^n$ configuration from the initial state |a J>, to the final state |b J′>can be described in terms of the oscillator strength by using the expression,

$$f_{cal}\left(aJ;bJ'\right)=\frac{8\pi^2 m\nu}{3h\left(2J+1\right)e^2n^2}\left[\chi_{ed}S_{ed}\left(aJ;bJ'\right)+\chi_{md}S_{md}\left(aJ;bJ'\right)\right] \quad (15.1)$$

where m is the mass of the electron, h the Planck's constant, ν is the frequency of the transition, J is the total angular momentum of the initial state, e the electron charge, and n is the refractive index of the host. $\chi_{ed}=\frac{n\left(n^2+2\right)^2}{9}$ and $\chi_{md}=n^3$ are the effective field correction at a well-localized center in a medium of refractive index n. S_{ed} and S_{md} are the line strengths for electric-dipole and magnetic-dipole transitions respectively, expressed by,

$$S_{ed}=e^2\sum_{t=2,4,6}\Omega_t\left|\left\langle aJ\left\|U^{(t)}\right\|bJ'\right\rangle\right|^2 \quad (15.2)$$

$$S_{md}=\frac{e^2\hbar^2}{4m^2c^2}\left|\left\langle aJ\left\|\overrightarrow{L}+2\overrightarrow{S}\right\|bJ'\right\rangle\right|^2 \quad (15.3)$$

$\langle\|U^{(t)}\|\rangle$ are the double-reduced matrix elements of the unit tensor operators which are considered to be independent of the host matrix and Ω_t are the JO parameters.

The calculated oscillator strengths can be compared with the experimental ones obtained from the absorption spectra by,

$$f_{\exp}=\frac{mc}{\pi e^2N}\int_{band}\alpha\left(\nu\right)d\nu \quad (15.4)$$

where N is the number of ions per unit volume and α(ν) is the absorption coefficient. Since the experimental oscillator strength contains electric-dipole and magnetic-dipole contributions, the latter has to be subtracted from the experimental one to obtain the electric-dipole contribution. The magnetic-dipole contribution, f_{md}, can be obtained from the equation $f_{md}=nf'$ [22], where n is the refractive index of the studied sample and f' is a quantity calculated based on the energy-level parameters for lanthanide aquo ions [23].

The JO parameters are derived from the electric-dipole experimental oscillator strengths by using a least squared fitting between experimental and calculated oscillator strengths. The magnetic dipole contribution is only present in transitions with $\Delta S=\Delta L=0$ and $\Delta J=0,\pm1$ [23].

The radiative transitions probability for electric- and magnetic-dipole transitions are given by,

$$A\left(aJ;bJ'\right)=A_{ed}+A_{md}=\frac{64\pi^4\nu^3}{3h\left(2J+1\right)c^3}\left[n\frac{\left(n^2+2\right)^2}{9}S_{ed}+n^3S_{md}\right] \quad (15.5)$$

The magnetic-dipole contributions can be calculated using the values given by Weber for LaF_3 [24] and correcting for the refractive index,

$$A_{md} = \frac{n}{n'} A'_{md} \tag{15.6}$$

where n and A_{md} are the values reported for LaF_3.

The radiative lifetime of an emitting level is related to the total spontaneous emission probability from this level by,

$$\tau_R = \left\{ \sum_{bJ'} A\left(aJ; bJ'\right) \right\}^{-1} \tag{15.7}$$

The emission branching ratio of a transition is defined by,

$$\beta = \frac{A\left(aJ; bJ'\right)}{\sum_{bJ'} A\left(aJ; bJ'\right)} \tag{15.8}$$

The experimental lifetimes and the radiative lifetimes can be related by,

$$\frac{1}{\tau_{\exp}} = \frac{1}{\tau_R} + W_{NR} = \frac{1}{\tau_R} + W_{MPH} + W_{ET} \tag{15.9}$$

where W_{NR} is the nonradiative probability. This nonradiative probability can be due to multiphonon relaxation, which depends on the host matrix, and/or energy transfer which is dependent on ion concentration.

Finally, one important parameter for laser applications and optical amplification is the emission cross-section. The stimulated emission cross-section can be obtained from the absorption spectrum by using the McCumber approach [25], which relates the absorption and emission cross-sections by,

$$\sigma_{em}(\nu) = \sigma_a(\nu) \exp\left[\frac{(\varepsilon - h\nu)}{KT}\right] \tag{15.10}$$

where σ_a and σ_{em} are the absorption and emission cross-sections respectively, ν is the photon frequency, ε is the net free energy required to excite one Er^{3+} ion from the $^4I_{15/2}$ to the $^4I_{13/2}$ state at temperature T, h is the Planck's constant, and K is the Boltzmann constant. The absorption cross-section is the absorption coefficient divided by the concentration of active ions and ε can be determined by using the simplified procedure provided in reference 26. The effective emission cross-section can also be calculated from the experimental emission spectrum and radiative transition probability by using the following expression [27],

$$\sigma_{eff} = \frac{\lambda_p^4}{8\pi n^2 c} \frac{1}{\Delta\lambda_{eff}} A\left(aJ; bJ'\right) \tag{15.11}$$

where c is the velocity of light, λ_p is the peak fluorescence wavelength, $\Delta\lambda_{eff}$ is the effective linewidth, A is the radiative transition probability of the emitting level, and n the refractive index. The effective linewidth of the emission is defined by,

$$\Delta\lambda_{eff} = \int \frac{I(\lambda)\, d\lambda}{I_{\max}} \tag{15.12}$$

15.3 Structural Characterization

Precursor oxyfluoride tellurite glass with a composition of 73.6 TeO_2–17.6 ZnO–8.8 ZnF_2 mol% doped with 1 wt% of ErF_3, which corresponds to $1.4 \cdot 10^{20}$ ions/cm^3, was prepared by the conventional melt-quenching technique. To nucleate a glass-ceramic (GC) phase a two step treatment was performed according to the values of the glass transition and crystallization temperatures ($T_g \approx 293$ °C and $T_c \approx 390$ °C respectively) [18]. The first treatment was done at 310 °C for 10 h, followed by a 3 h treatment at 340 °C, which is below that of the onset of crystallization.

The microstructure of the samples and chemical composition of the nanocrystals have been analyzed by Transmission Electron Microscopy (TEM) and Energy Dispersive X-ray spectroscopy (EDX). TEM analysis clearly demonstrates the formation of nanocrystals in the heat treated sample as it is shown in Fig. 15.1a. They present a dendritic structure with typical sizes of 45 ± 10 nm and clear lattice fringes. The Fast Fourier Transform (FFT) of this image in Fig. 15.1b shows different brilliant spots in the reciprocal space which can be indexed according to the planes of ErF_3 crystals obtained in the [101] direction. This analysis was performed based on the compositional profile obtained from EDX spectroscopy. The EDX analysis of the nanocrystals (Fig. 15.2) shows intense peaks corresponding to F and

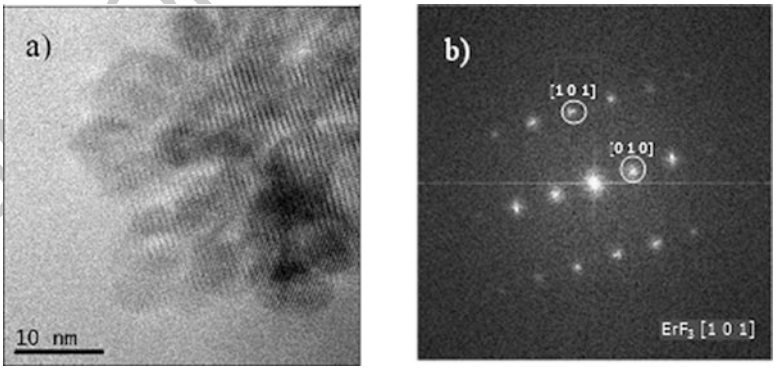

Fig. 15.1 (**a**) HRTEM image of the GC sample. (**b**) Fast Fourier Transform (FFT) image indexed according to the ErF_3 structure

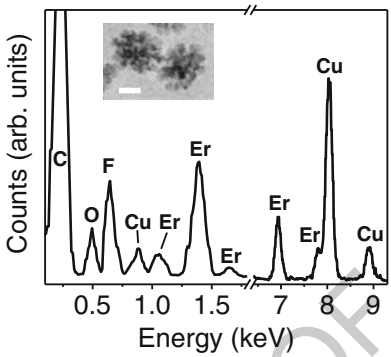

Fig. 15.2 EDX spectrum in the energy ranges 0–1.8 and 6.5–9.3 keV of the nanocrystals observed in the GC sample. The elements responsible for the peaks observed are indicated. The inset shows a TEM image of two of these nanocrystals, where the horizontal line corresponds to 20 nm

Er in addition to those associated to the C layer of the replica and the Cu grid (C, O, and Cu). The absence of peaks related to Zn or Te suggests that the nanocrystals are formed by ErF_3.

15.4 Influence of the Nanocrystals on the Luminescence Properties of Er^{3+} Ions

15.4.1 Absorption Properties

The influence of the nanocrystals on the spectroscopic properties of Er^{3+} ions in glass-ceramic samples based on fluorotellurite glasses has been studied by using absorption and steady-state and time-resolved laser spectroscopy. The absorption spectra of the glass (GS) and glass-ceramic (GC) samples are displayed in Fig. 15.3. The absorption bands are assigned to the transitions from the $^4I_{15/2}$ ground state to the excited states of Er^{3+} ions. Due to the absorption of the host in the UV, some transitions are not observed. As can be seen, there are some difference between both spectra due to the presence of the nanocrystals (NCs). The absorption edge is shifted to longer wavelengths in the GC sample due to the scattering of short wavelength light by the NCs present in this sample. Moreover, the intensity of the hypersensitive transition $^4I_{15/2} \rightarrow {}^2H_{11/2}$ is strongly reduced in the glass-ceramic sample which indicates that the ligand field around Er^{3+} ions has changed as a consequence of the heat treatment. The strength of the hypersensitive transitions is greatly affected by the environment of rare earth ions. Ligand polarizability as well as an asymmetric surrounding environment increases the intensity of hypersensitive transitions of RE ions [28–30]. Another evidence of the incorporation of Er^{3+} ions in the nanocrystals is the splitting of the inhomogeneously broadened absorption bands in the absorption spectrum of the GC sample. As an example, the inset in Fig. 15.3 shows a detail of the $^4I_{15/2} \rightarrow {}^4I_{13/2}$ absorption band for the glass and GC samples.

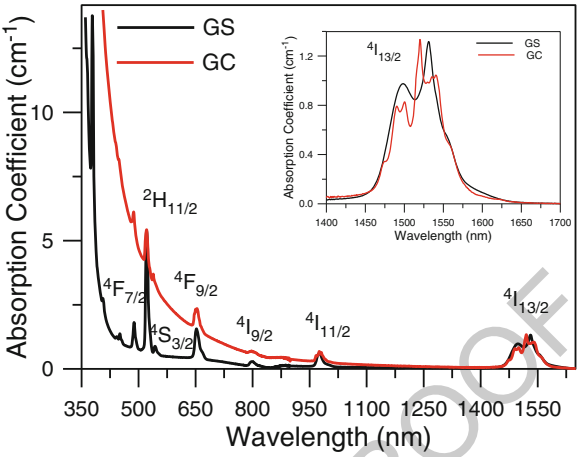

Fig. 15.3 Room temperature absorption spectra for precursor glass and glass-ceramic samples. The inset shows the detail of the $^4I_{15/2} \rightarrow {}^4I_{13/2}$ absorption bands

Table 15.1 Judd-Ofelt parameters and r.m.s. deviation for precursor glass (GS) and glass ceramic (GC) samples

Sample	Ω_2 ($\times 10^{-20}$)	Ω_4 ($\times 10^{-20}$)	Ω_6 ($\times 10^{-20}$)	r.m.s.	
GS	4.71	1.57	1.13	$3.24 \cdot 10^{-7}$	t3.1
GC	1.28	1.04	1.00	$3.47 \cdot 10^{-7}$	t3.2

The absorption spectra have been used to calculate the radiative transition probabilities, the radiative lifetimes, and branching ratios of the emissions by using the JO intensity parameters. From these spectra the experimental oscillator strengths have been calculated and following the procedure described in Sect. 2, the theoretical oscillator strengths and the JO parameters of Er^{3+} ions in the glass and glass-ceramic samples. The values are displayed in Table 15.1. The matrix elements given by Carnall et al [23] have been used in the calculation. The low value of the root mean square (rms) indicates a good agreement between the experimental and calculated oscillator strengths.

The value of Ω_2 in the GC sample is lower than in the GS, which means that the heat treatment induces a reduction in the degree of covalency in the rare-earth site. It is well known that Ω_2 is most sensitive to local structure and its value is indicative of the amount of covalent bonding between RE ions and ligand anions. The decrease of Ω_2 further confirms the incorporation of Er^{3+} ions into the fluoride NCs. Moreover, the sum of the JO parameters decreases for the GC sample due to the decrease of covalency of the chemical bond between the Er^{3+} ion and the ligand anions. This is in accordance with reported results that predict that the sum decrease in the order oxide > oxyfluoride > fluoride. In addition, the Ω_2 parameter is closely related to the hypersensitive transitions. The more intense the hypersensitive transition is, the larger the value of Ω_2 is. The lower value of this parameter in the heat treated sample is in agreement with the decrease of the strength of the hypersensitive transition $^4I_{15/2} \rightarrow {}^2H_{11/2}$ which indicates the variation of the local structure around the Er^{3+} ions and further confirms their incorporation into the nanocrystals.

The JO parameters have been used to calculate the radiative transition probabilities and radiative lifetimes. The radiative lifetimes of level $^4I_{13/2}$ are 3.23 and 3.73 ms for the GS and GC sample respectively.

15.4.2 Near Infrared Emission

The room temperature near infrared emission spectra have been obtained by exciting at 801 nm in the $^4I_{9/2}$ level with a Ti-sapphire ring laser. The fluorescence was analyzed with a monochromator and the signal detected with a photomultiplier and finally amplified by a standard lock-in technique. After excitation of level $^4I_{9/2}$, the next lower levels are populated by multiphonon relaxation. Two emission bands were observed at around 980 and 1530 nm, which correspond to transitions from $^4I_{11/2}$ and $^4I_{13/2}$ levels to the ground state respectively. Figure 15.4 shows the emission spectra corresponding to the $^4I_{13/2} \rightarrow {}^4I_{15/2}$ transition. The spectrum of the GC sample shows a more resolved structure with seven Stark components. Moreover, the effective bandwidth is reduced from 73.4 nm in the Gs to 64 nm in the GC sample probably due to the reduction of inhomogeneous broadening.

Figure 15.5 shows the absorption and emission cross-sections obtained for the GC sample by using the McCumber approach together with the normalized measured emission spectrum. The stimulated emission cross-section has a value of $8.9 \cdot 10^{-21}$ cm^2, similar to the one found in the glass sample ($8.8 \cdot 10^{-21}$ cm^2) [16] and higher than those found in other fluorotellurite glass-ceramics [31].

The comparison of the excitation spectra of the $^4I_{15/2} \rightarrow {}^4I_{9/2}$ transition obtained by collecting the luminescence at 1540 nm for the glass and glass-ceramic samples also confirms the incorporation of Er^{3+} ions in the nanocrystals. As can be seen in

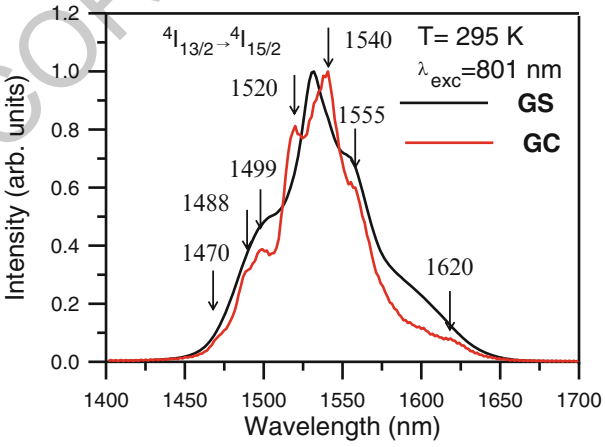

Fig. 15.4 Room temperature emission spectra obtained under excitation at 801 nm in the glass and glass-ceramic samples

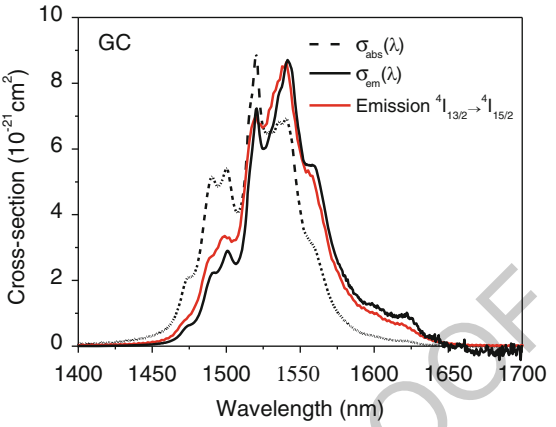

Fig. 15.5 Absorption and emission cross-sections of the $^4I_{13/2} \leftrightarrow {}^4I_{15/2}$ transitions for the GC sample together with the normalized emission spectrum

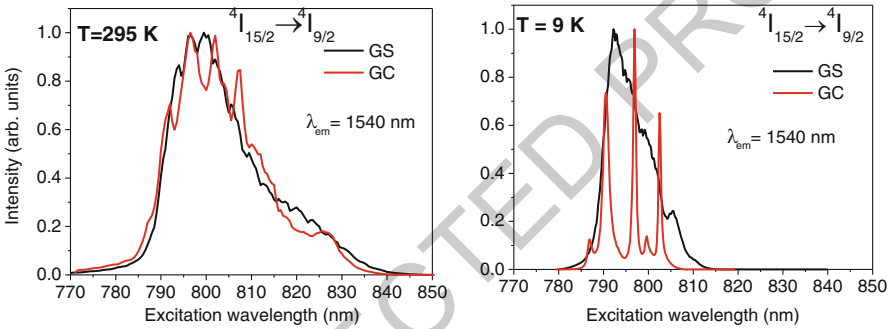

Fig. 15.6 Excitation spectra of the $^4I_{15/2} \rightarrow {}^4I_{9/2}$ transition obtained by collecting the luminescence at 1540 nm in the glass and glass-ceramic samples at 295 K and 9 K

Fig. 15.6, the spectrum corresponding to the GC sample shows well defined peaks not observed in the excitation spectrum of the glass sample. This is more evident from the low temperature excitation spectrum of the GC sample which shows narrow peaks according with the presence of Er^{3+} ions in a crystalline environment.

The experimental decays of luminescence from levels $^4I_{11/2}$ and $^4I_{13/2}$ were obtained at room temperature for both samples by exciting at 801 nm in level $^4I_{9/2}$ by using a Ti-sapphire laser pumped by a pulsed frequency doubled Nd:YAG laser (9 ns pulse width). The decay from level $^4I_{13/2}$ shows, in both samples, an initial rise time due to the population from the higher $^4I_{11/2}$ level. Figure 15.7 shows the experimental decay curves for GC and GS samples. The decay of the glass sample can be described by a single exponential function with a lifetime of 3.6 ms, however the experimental decay of the GC sample is well described by a double exponential function with lifetimes of 1.2 and 3.1 ms which suggest contributions from different environments around Er^{3+} ions. In the GC, a fraction of Er^{3+} ions remains in a glass environment while the rest is forming NCs. The reduction in lifetimes after heat treatment has been previously reported [32] and attributed to the segregation

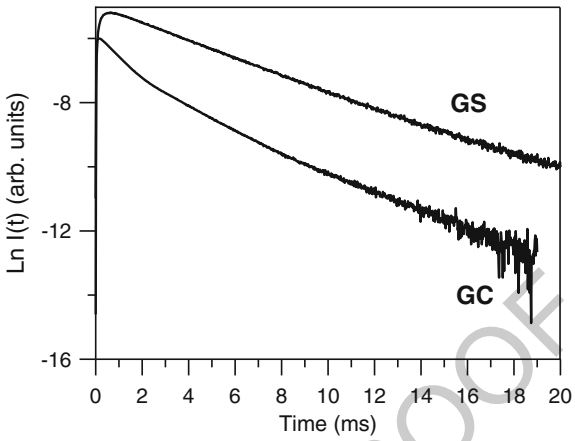

Fig. 15.7 Semilogarithmic plot of the fluorescence decays of the $^4I_{13/2}$ level for precursor glass and glass-ceramic samples obtained after excitation at 801 nm

of the rare-earth ions into the crystalline phase which reduces Er^{3+}-Er^{3+} distances. Shorter distances between Er^{3+} ions favour dipole-dipole energy transfer between them, which increases non-radiative rates and reduces the lifetime of level $^4I_{13/2}$. A similar behavior is observed for the lifetime value of the $^4I_{11/2}$ level which is reduced from 420 μs in the glass sample to 220 μs in GC sample.

15.4.3 Upconversion Emission

Up-conversion (UC) is an anti-Stokes process that converts the absorbed lower energy photons, usually in the NIR range, into higher energy photons in UV, visible, or shorter NIR ranges. UC can occur mainly by two fundamental mechanisms: (i) excited state absorption (ESA); (ii) energy transfer upconversion (ETU). In the case of ESA, excitation involves sequential absorptions of pump photons by a single ion. This mechanism requires a nearly equal separation for the first and second steps, as well as the long lifetime of the intermediate level. In an ETU process, two ions interact, one of then loses energy and goes to the ground state whereas the other one gains energy and goes to the upper level. The UC efficiency of an ETU process is strongly dependent on the active ions concentration. In contrast to ETU, the efficiency of an ESA process is independent of the dopant concentration, because ESA involves sequential excitation in the same ion.

Visible upconversion emission has been observed for both glass and GC samples at room temperature under continuous wave (cw) and pulsed laser excitation in resonance with the $^4I_{9/2}$ level. The upconverted emission spectra obtained under cw excitation were measured by using a Ti-sapphire ring laser. Cut-off filters were used to remove the pumping radiation. Figure 15.8a shows the upconversion emission spectra corresponding to the glass and glass-ceramic samples. The upconversion emission of the glass sample shows the characteristic green emission attributed

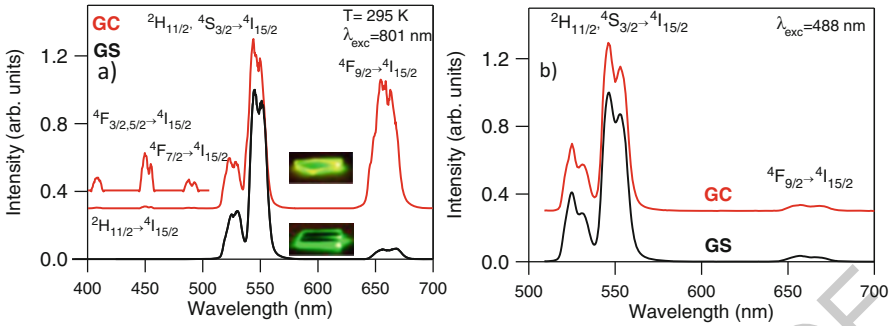

Fig. 15.8 Visible emission obtained (**a**) under 801 nm and (**b**) under 488 nm excitation for the glass and glass-ceramic samples

to the transitions from the two thermallized levels ($^2H_{11/2}$, $^4S_{3/2}$) together with a weak red emission from the $^4F_{9/2}$ level. However, the spectrum of the GC sample shows in addition to the green and red emissions very weak blue emissions from higher levels which do not appear in the upconversion emission of the glass sample. As can be seen, the emission bands are better resolved in the GC spectrum in agreement with the incorporation of Er^{3+} ions in the crystalline phase. Moreover, the intensity of the red emission increases significantly in the GC sample. This increase of the red emission, not observed in the spectra obtained by exciting at 488 nm (Fig. 15.8b), indicates that after NIR excitation, level $^4F_{9/2}$ is populated by energy transfer processes in addition to multiphonon relaxation from level $^4S_{3/2}$. This behavior could be associated to a higher concentration of Er^{3+} ions in the nanocrystals, which reduces the Er^{3+}-Er^{3+} distances and increases the probability of energy transfer processes [33, 34].

To investigate the excitation mechanisms for populating the $^4S_{3/2}$ and $^4F_{9/2}$ levels after IR excitation in the GC sample, we have measured the upconverted emission intensities for different pumping powers. The upconversion emission intensity (I_{em}) depends on the incident pump power (P_{pump}) according to the relation $I_{em} \propto (P_{pump})^n$, where n is the number of photons involved in the pumping mechanism. Figure 15.9 shows a logarithmic plot of the integrated emission intensity of the upconverted green and red fluorescence as a function of the pump laser intensity. The dependence in both cases is nearly quadratic which indicates a two photon (TP) upconversion process to populate the $^4S_{3/2}$ and $^4F_{9/2}$ levels. This process may be associated with excited state absorption and/or energy transfer upconversion.

As it is well known, the time evolution of the upconversion luminescence after an excitation pulse provides an useful tool in discerning which the operative mechanism is. The radiative ESA process occurs during the excitation pulse and leads to an immediate decay of the upconversion luminescence after excitation. Upconversion by energy transfer leads to a time-dependent emission that shows a rise of the upconverted population after the laser pulse, followed by a decay of

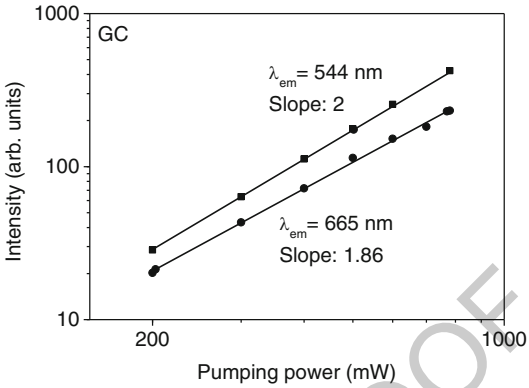

Fig. 15.9 Logarithmic plot of the integrated intensities of the upconverted emission from $^4S_{3/2}$ (544 nm) and $^4F_{9/2}$ (665 nm) levels obtained under excitation at 801 nm

the population, with a lifetime longer than the one after direct excitation. The rise and decay times are determined by both the intermediate and the upper excited state lifetimes. This distinction is possible when the pump pulse width is much shorter than the time constant of the relevant energy transfer step.

According to the energy level diagram of Er^{3+} ion in the GC sample, the $^4S_{3/2}$ level can be populated by ESA and/or ETU in the case of the green emission(Fig. 15.10). In the first case, the absorption of an IR photon excites the electrons to the $^4I_{9/2}$ level, then multiphonon relaxation populates the next lower level, and the absorption of a second IR photon promotes the electrons to the $^4F_{3/2,5/2}$ levels from where $^4S_{3/2}$ level is reached by nonradiative relaxation. Part of the excitation energy in the $^4I_{11/2}$ level further relaxes, radiatively and nonradiatively to level $^4I_{13/2}$ and ESA from $^4I_{13/2}$ to $^2H_{11/2}$ can occur. This last process is nearly resonant. Another possibility is an energy transfer process which involves the interaction between two Er^{3+} ions in the $^4I_{11/2}$ level. In this process one ion gains energy and reaches level $^4F_{7/2}$, whereas the other one loses energy and goes to the ground state.

The lifetime behavior of the upconverted green emission suggests that both processes ESA and ETU are present. Figure 15.11a shows the decays of the green emission obtained by exciting at 488 and 801 nm respectively for the GC sample. In both cases, the decays can be described to a good approximation by two components. The fast one has a lifetime of 36 and 41 μs for the 488 and 801 nm excitation respectively but the lifetime of the long component (129 μs), is longer than the one obtained by direct excitation (107 μs). The observation of the instantaneous rise after the 9 ns pulse excitation indicates the presence of an ESA process; however, the longer lifetime of the slow component after IR excitation indicates that an additional ETU process is also necessary to describe the lifetime of the decay. The lifetime of the long component (129 μs) is about half the lifetime of the $^4I_{11/2}$ level (220 μs), which suggests that the upconversion green emission from level $^4S_{3/2}$ can be produced by the interaction between two Er^{3+} ions in the $^4I_{11/2}$ level via the transitions ($^4I_{11/2} \rightarrow {}^4I_{15/2}$) and ($^4I_{11/2} \rightarrow {}^4F_{7/2}$).

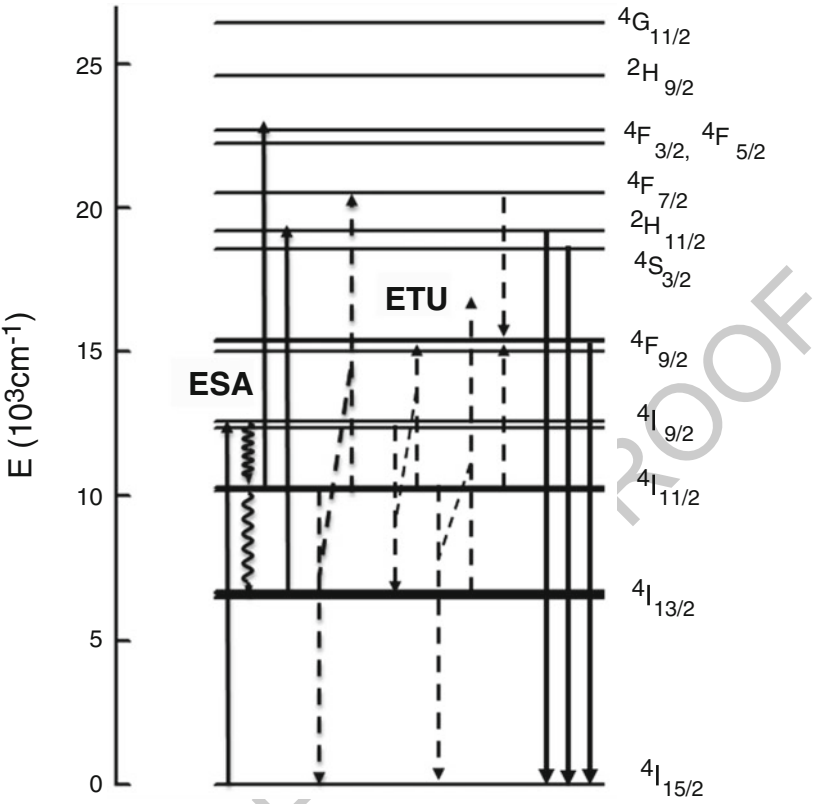

Fig. 15.10 Energy level diagram of Er^{3+} ions in the GC sample and possible upconversion mechanisms

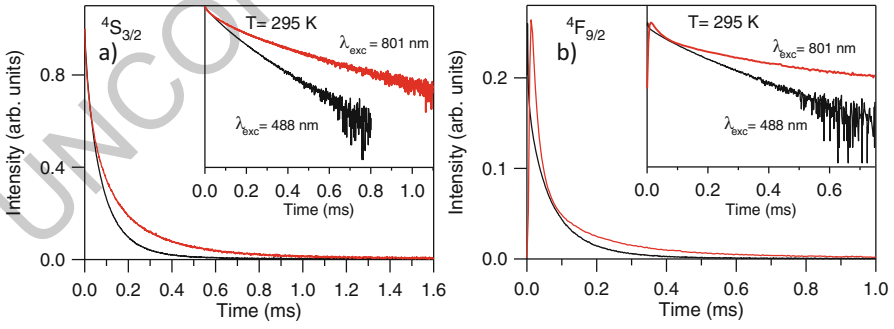

Fig. 15.11 Semilogarithmic plot of the experimental decay curves of the (**a**) *green* ($^4S_{3/2}$) and (**b**) *red* ($^4F_{9/2}$) emissions under excitation at 488 nm (*black line*) and 801 nm (*red line*) for the GC sample

Instead, the time evolution of the upconverted red emission confirms that the $^4F_{9/2}$ level is populated by ETU processes. As an example, the time evolution of the red emission obtained under excitation at 801 nm and 488 nm for the GC sample is shown in Fig. 15.11b. In both cases, the decays can be described by two components. The fast one (∼21 μs) is similar for both excitation wavelengths whereas the lifetime of the slow component increases from 89 μs to 183 μs when the excitation wavelength changes from 488 nm to 801 nm. Moreover, there is an initial rise time of about 15 μs. The presence of a rise time together with the lengthening of the slow component of the decay supports the hypothesis that ETU processes are populating level $^4F_{9/2}$. According to the energy level diagram of Er^{3+} ions in the GC sample (Fig. 15.10), there are different ETU processes to populate the $^4F_{9/2}$ level. This level can be populated via ($^4I_{9/2} \rightarrow {}^4I_{13/2}$) and ($^4I_{11/2} \rightarrow {}^4F_{9/2}$) transitions and/or ($^4I_{11/2} \rightarrow {}^4I_{15/2}$) and ($^4I_{13/2} \rightarrow {}^4F_{9/2}$). There exists another possible process for populating level $^4F_{9/2}$ in which two Er^{3+} ions interact, one of them in level $^4I_{11/2}$ and the other one in level $^4F_{7/2}$, going both to level $^4F_{9/2}$. By considering that the lifetime of a higher-energy level excited by ETU reflects those of the intermediate levels from which upward excitation occurs, and that the long component of the decay of the red emission after excitation at 801 nm is very close to the lifetime of level $^4I_{11/2}$, the ($^4I_{9/2} \rightarrow {}^4I_{13/2}$);($^4I_{11/2} \rightarrow {}^4F_{9/2}$) and ($^4F_{7/2} \rightarrow {}^4F_{9/2}$);($^4I_{11/2} \rightarrow {}^4F_{9/2}$) processes seem to be the likeliest ones to explain the population of the $^4F_{9/2}$ level by ETU.

15.5 Conclusions

Transparent glass-ceramics containing ErF_3 nanocrystals have been prepared by suitable thermal treatment of an Er^{3+}- doped 73.6 TeO_2–17.6 ZnO–8.8 ZnF_2 mol% fluorotellurite glass.

The comparison of the fluorescence properties of Er^{3+}-doped precursor glass and glass-ceramic confirms the successful incorporation of the rare-earth into the nanocrystals. The strong reduction of the Ω_2 JO parameter and the intensity of the hypersensitive transition $^4I_{15/2} \rightarrow {}^2H_{11/2}$ in the heat treated sample indicate that Er^{3+} ions are in a crystalline environment. The $^4I_{13/2}$ decay in the glass-ceramic sample can be described by two single exponential functions which suggests that a fraction of Er^{3+} ions are forming nanocrystals while the rest remains in a glass environment. Moreover, the emission lifetime is shorter than in the glass sample probably due to the segregation of the Er^{3+} ions into the crystalline phase which reduces Er^{3+}-Er^{3+} distances and increases energy transfer processes.

The presence of ErF_3 nanocrystals has a strong effect in the upconverted red emission from $^4F_{9/2}$ level. This emission increases significantly as compared with the green one in the GC sample. The time evolution of the upconverted red emission suggests that ETU processes are responsible for the increase of this emission in the glass-ceramic sample.

Acknowledgments We deeply acknowledge A. Tomas from the National Centre for Metallurgical Research (CENIM, CSIC) and A. Ruiz-Caridad from the Laboratory of Electron Nanoscopies (LENS, University of Barcelona) for TEM sample preparation and HRTEM analysis, respectively. This work was supported by the Spanish Government MEC under Projects No. TEC2012-38901-C02-01 and MAT2013-48246-C2-2-P and Basque Country Government IT-659-13 and IT-943-16. R. Morea acknowledge a FPI grant from the Spanish Government (BES-2010-038084).

References

AQ2

1. Dejneka, M. J. (1998). *MRS Bulletin, 11*, 57.
2. Wang, Y., & Ohwaki, J. (1993). *Applied Physics Letters, 63*, 3268.
3. Chen, D., Yu, Y., Huang, P., Lin, H., Shan, Z., & Wang, Y. (2010). *Acta Materialia, 58*, 3035.
4. Luo, Q., Qiao, X., Fan, X., Yang, H., Zhang, X., Cui, S., Wang, L., & Wang, G. (2009). *Journal of Applied Physics, 105*, 043506.
5. Velazquez, J. J., Rodrigu[illegible] D., Yanes, A. C., del-Castillo, J., & Mendez-Ramos, J. (2010). *Journal of Applied Physics, 108*, 113530.
6. Secu, M., Secu, C. E., Polosan, S., Aldica, G., & Chica, C. (2009). *Journal of Non-Crystalline Solids, 355*, 1869.
7. Sun, X., Gu, M., Huang, S., Jin, X., Lui, X., Liu, B., & Ni, C. (2009). *Journal of Luminescence, 129*, 773.
8. Qiao, X., Fan, X., & Wang, M. (2006). *Scripta Materialia, 55*, 211.
9. Luo, Q., Fan, X., Qiao, X., Yang, H., Wang, M., & Zhang, X. (2009). *Journal of the American Ceramic Society, 92*, 942.
10. Goncalves, M. C., Santos, L. F., & Almeida, R. M. (2002). *Comptes Rendus Chimie, 5*, 845.
11. de Pablos-Martín, A., Durán, A., & Pascual, M. J. (2012). *International Materials Reviews, 57*, 165.
12. El-Mallawany, R. A. H. (2001). *Tellurite glasses handbook-physical properties and data*. Boca Raton: CRC Boca Raton.
13. Mori, A. (2002). *IEEE Journal of Lightwave Technol., LT-20*, 822.
14. Richards, B., Tsang, Y., Binks, D., Lousteau, J., & Jha, A. (2008). *Optics Letters, 33*, 402.
15. Sidebottom, D. L., Hruschka, M. A., Potter, B. G., & Brow, R. K. (1997). *Applied Physics Letters, 71*, 1963.
16. Miguel, A., Morea, R., Gonzalo, J., Arriandiaga, M. A., Fernandez, J., & Balda, R. (2013). *Journal of Luminescence, 140*, 38.
17. Yu, C., Zhang, J., Wen, L., & Jiang, Z. (2007). *Materials Letters, 61*, 3644.
18. Miguel, A., Morea, R., Arriandiaga, M. A., Hernández, M., Ferrer, F. J., Domingo, C., Fdez-Navarro, J. M., Gonzalo, J., Fernandez, J., & Balda, R. (2014). *Journal of the European Ceramic Society, 34*, 3433.
19. Russell, H. N., & Saunders, F. A. (1925). *Astrophysical Journal, 61*, 38.
20. Judd, B. R. (1962). *Physics Review, 127*, 750.
21. Ofelt, G. S. (1962). *Journal of Chemical Physics, 37*, 511.
22. Carnall, W. T., Fields, P. R., & W[illegible]ne, B. G. (1968). *Journal of Chemical Physics, 49*, 4412.
23. Carnall, W. T., Fields, P. R., & Rajnak, K. (1968). *Journal of Chemical Physics, 49*, 4424.
24. Weber, M. J. (1967). *Physics Review, 157*, 262.
25. McCumber, D. E. (1964). *Physics Review, 136*, A954.
26. Miniscalco, W. J., & Quimby, R. S. (1991). *Optics Letters, 16*, 258.
27. Weber, M. J., Ziegler, D. C., & Angell, C. A. (1982). *Journal of Applied Physics, 53*, 4344.
28. Ebendorff-Heidepriem, H., Ehrt, D., Bettinelli, M., & Speghini, A. (1998). *Journal of Non-Crystalline Solids, 240*, 66.
29. Jorgensen, C. K., & Reisfeld, R. (1983). *Journal of Less-Common Metals, 93*, 107.

30. Tanabe, S., Ohyagi, T., & Soga, N. (1992). *Physical Review B, 46*, 3305–3310.
31. Jlassi, I., Elhouichet, H., Hraiech, S., & Ferid, M. (2012). *Journal of Luminescence, 132*, 832.
32. Dantelle, G., Mortier, M., Patriarche, G., & Vivien, D. (2006). *Journal of Solid State Chemistry, 179*, 1995.
33. Balda, R., García-Revilla, S., Fernández, J., Seznec, V., Nazabal, V., Zhang, X. H., Adam, J. L., Allix, M., & Matzen, G. (2009). *Optical Materials, 31*, 760.
34. Balda, R., García-Adeva, A. J., Fernández, J., & Fdez-Navarro, J. M. (2004). *Journal of the Optical Society of America B, 21*, 744.

AUTHOR QUERIES

AQ1. Please confirm the affiliation details.
AQ2. Please provide article title for all the references.